Düzce University Journal of Science & Technology

Research Article

Improvement and Analysis of Phase-Phase Failure of Double Feed Induction Generator Using Maximum Power Monitoring Method

Mustafa DURSUN [a,*]

[a] *Elektrik Elektronik Mühendisliği Bölümü, Mühendislik Fakültesi, Düzce Üniversitesi, Düzce, TÜRKİYE*
** Sorumlu yazarın e-posta adresi: mustafadursun@duzce.edu.tr*
DOI: 10.29130/dubited.1052660

ABSTRACT

This study presents an analysis and control method for the doubly fed induction generator (DFIG) based wind energy production under the conditions of sudden grid voltage dips. The control aims are as follows: limiting the rotor currents, suppressing the fluctuations in the torque and suppressing the dc-link voltage fluctuation via the converter controls and ensuring maximum power point tracking. Rotor side converter (RSC) and grid side converter (GSC) structures have been given in the article and their limitations have been specified. Maximum power tracking control block has also been included in the system and its structure has been given. In this study; while RSC is controlled in a way that it will suppress the fluctuations in the torque and rotor currents, GSC is controlled in a way that it will suppress the fluctuations in dc-link voltage while taking the rotor power impact into consideration. Crowbar unit has been used in the rotor side to minimize these impacts. This unit is activated at the moment when a grid dip occurs and deactivates the RSC side. In this way, RSC side will not be affected by the high current fluctuations. The detailed results of the study were carried out in the MATLAB/Simulink environment, and the effectiveness of the proposed method was supported by the graphic results.

Keywords: *DFIG, Voltage dips, Rotor side converter (RSC), Grid side converter (GSC), MATLAB/Simulink.*

Maksimum Güç İzleme Yöntemi Kullanılan Çift Beslemeli Asenkron Generatörün Faz-Faz Arızasının İyileştirilmesi ve Analizi

ÖZ

Bu çalışma, ani şebeke gerilim düşüşleri koşullarında çift beslemeli endüksiyon generatörü (ÇBAG) tabanlı rüzgar enerjisi üretimi için bir analiz ve kontrol yöntemi sunmaktadır. Kontrol amaçları şunlardır: Rotor akımlarının sınırlandırılması, torktaki dalgalanmaların bastırılması ve konvertör kontrolleri aracılığıyla dc-link voltaj dalgalanmasının bastırılması ve maksimum güç noktası takibinin sağlanması. Makalede rotor tarafı dönüştürücü (RTD) ve şebeke tarafı dönüştürücü (ŞTD) yapıları verilmiş ve sınırlamaları belirtilmiştir. Maksimum güç takip kontrol bloğu da sisteme dahil edilmiş ve yapısı verilmiştir. Bu çalışmada; RTD, tork ve rotor akımlarındaki dalgalanmaları bastıracak şekilde kontrol edilirken, ŞTD, rotor güç etkisi dikkate alınarak dc-bara gerilimindeki dalgalanmaları bastıracak şekilde kontrol edilir. Bu etkileri en aza indirmek için rotor tarafında crowbar ünitesi kullanılmıştır. Bu ünite, şebeke geriliminde bir düşüş meydana geldiği anda etkinleştirilir ve RTD tarafını devre dışı bırakır. Bu sayede RTD tarafı yüksek akım dalgalanmalarından etkilenmeyecektir. Çalışmanı detaylı sonuçları MATLAB/Simulink ortamında gerçekleştirilerek, önerilen metodun etkinliği grafik sonuçları ile desteklenmiştir.

Anahtar Kelimeler: *ÇBAG, Gerilim düşümü, Rotor tarafı dönüştürücü (RTD), Şebeke tarafı dönüştürücü (ŞTD), MATLAB/Simulink.*

Received: 03/01/2022, Revised: 15/01/2013, Accepted: 09/02/2022

I. INTRODUCTION

When compared to other energy sources; wind energy being from the renewable energy sources is an energy which is clean and produced by using directly the wind in the nature with no cost of raw material and transportation. Wind turbines are separated into two groups as constant-speed and variable-speed according to their operational principles when the speed of the wind is taken as the basis. Constant speed wind turbines are used in the places where the wind speed is constantly at a certain range (± 1%) and are connected to the grid directly. The variable speed wind turbines are convenient for the places where the wind speed is variable (± 30%) and are connected to the grid with the help of a grid interface [1]. The wind turbines used today are mostly produced as variable speed ones; because, the kinetic energy owned by the wind is not constant and variable speed wind turbines are used to be able to transmit this variable energy owned by the wind to the output in maximum level [2]. Doubly Fed Induction Generator (DFIG) being one of the types of generators used in the variable speed wind turbines is widely used in recent years due to its advantages such as being able to operate within ±30% speed range of the synchronous speed and the converter power of the power electronics to be by the ratio of 30% of the generator power [3]. DFIG consists of two different windings as stator and rotor which are electrically insulated from each other. While the stator windings of DFIG are directly connected to the grid, the rotor windings are connected to the grid upon the converter of power electronics consisting of two voltage-based inverters in which there could be bidirectional current flow [4].

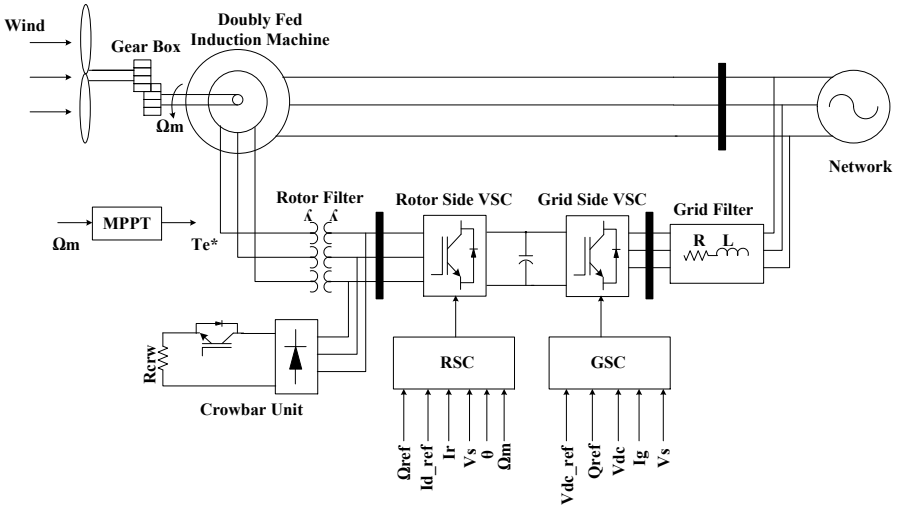

Figure 1. *Grid connected control model of DFIG based wind türbine.*

The schematic model of DFIG system is shown in Figure 1. The inverter in rotor side inspects the active and reactive power of the stator and provides the reactive power needed by the generator. The grid side inverter keeps the DC bus bar voltage stable [5].

LVRT method known as low voltage rehabilitation method is frequently used to ensure stability in grid failures [22-26]. The advantages such as the partial operation of the power converters and variable speed processes provide opportunities for DFIG to be commonly used in the wind energy conversion system [6]. In addition; the stator of DFIG is directly connected to the grid; for this reason, its delicacy against grid failures increases. High stator current may occur due to the voltage failures in the grid [7, 8, 9, 10].

Many LVRT techniques have been suggested in the literature to develop the LVRT capacity of DFIG system have generally been given place [11,12,13]. Many converters [11]-[14] are recommended for low voltage recovery in a DFIG system. Among these, the use of crowbars is recommended to limit the high currents and voltages in the rotor currents of DFIG for wind turbines used in industry in most of the application-oriented protection methods [15] - [16]. In case of faults occurring in the grid, this crowbar circuit is triggered and the rotor side control unit keeps and maintains the rotor current between the specified limits. As a result, DFIG works as a generator that draws reactive power from the grid

during grid faults [17]. In the case of LVRT [12] - [18] some advanced crowbar circuits have been proposed to increase the performance of the DFIG system. The impact of voltage dips on wind turbine generator was worked in [11]. The behavior of DFIG during the balanced dips was worked in the references [7,9,10]. The theoretical analysis ways in [7,9,10] are applied in wide range in the related studies, but how DFIG reacts has not been examined when a dip occurs at the moment of the maximum power tracing [12].

In studies in the literature, one of the biggest problems for LVRT is the occurrence of overcurrents in transient analysis. While determining the maximum power point in wind turbines, the use of the crowbar unit becomes very important against these temporary situations. In this study, we developed the crowbar unit in order for the wind turbine to work effectively in case of failure at maximum power points, as well as maximum power monitoring.

In this study, in chapter 2 maximum power point tracking (MPPT) algorithm, in chapter 3 the model of DFIG system and grid connected operation by vector control technique, crowbar unit and in the last chapter the response to the voltage dip during MPPT was investigated. Detailed graphics are given.

II. MODELLING

DFIG system contains back-to-back converters together with a wind turbine, generator, grid side control and rotor side control systems and is connected to the grid upon the transformer (as seen in Figure 1). The control system consists of two systems: wind turbine (WT) control and converter controls. The WT adjusts the rotor speed of the DFIG by generating a reference torque value. It also controls the mechanical power of the wind turbine according to the angle of inclination. The two-level control strategy was used above and below the nominal speed [19].

A. WIND TURBINE AERODYNAMIC MODEL

The energy coming from the wind is mechanically caught by the wings in the DFIG based variable speed wind turbines and after that, it is converted into electrical energy by DFIG and finally, this energy is transmitted to the mains [20]. Momentum theory is used to examine the behavior of the wind turbine. Power could be attained from wind under some ideal assumptions.

$$P_t = \frac{1}{2}\rho\pi R^2 V_w^3 C_p \quad (1)$$

Here; ρ is the air density. R is the wing diameter of the wind turbine. V_w is the wind speed and C_p is a non-dimensional parameter expressing the activity of the wind turbine for transforming the kinetic energy of the wind into mechanic energy. This coefficient is a function of the wind speed, rotation speed of the wind turbine Ω_t and the pitch angle β for a certain wind turbine. C_p is generally given as $C_p = f(\lambda,\beta)$ as a λ function of terminal velocity.

$$\lambda = \frac{\Omega_t R}{V_w} \quad (2)$$

Theoretically, the maximum value of C_p is given with Betz limits: $C_{p\_theo\_max} = 0.44$ Figure 2 shows the value of the C_p curve as the graphics used in this study.

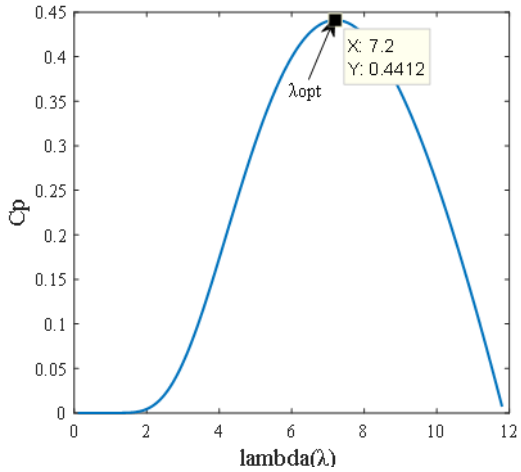

Figure 2. *Cp coefficient of the wind turbine used in the study.*

It is seen in Figure 2 that the maximum power coefficient is 0.44 and optimum tip speedratio is 7.2 in the graphics of the power coefficient as a function of the tip speed ratio for the equation 2.

A.1. Turbine Control

The general control model of wind turbine is shown in Figure 1. The rotor side control of DFIG is conducted by the rotor side converter. However; the PI regulator conducting the speed control here could be deactivated. In this way; torque references are generated with this improved control structure, MPPT (maximum power point tracking) algorithm. Grid-side converter transmits the power generated to the grid through the rotor of the DFIG, and also controls the DC bus. In Figure 1, the torque generated by DFIG is set to a constant speed according to a certain value. When MPPT is used as in Figure 3 (operation in C_{p_max}), an indirect speed control is carried out by benefitting from the fact that the produced power follows a cubic relation with the speed.

$$V_w = \frac{R\Omega_t}{\lambda_{opt}} \Rightarrow P_t = \frac{1}{2}\rho\pi R^2 \left(\frac{R\Omega_t}{\lambda_{opt}}\right)^3 C_{p_{max}}$$

$$\Rightarrow \begin{cases} P_t = k_{opt}\Omega_t^3 \\ k_{opt} = \frac{1}{2}\rho\pi R^5 \frac{C_{p\_max}}{\lambda_{opt}^3} \end{cases} \quad (3)$$

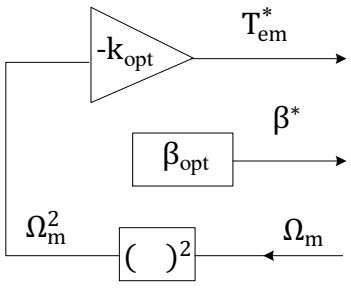

Figure 3*. Indirect speed controlled MPPT*

The output mechanic moment is specified as in [20] for the wind turbine.

$$T_m = \frac{1}{2}\rho A R^3 V_v^2 C_t \tag{4}$$

Here; ρ is the air intensity, A is the wing sweeping area, R is the rotor angle of the wind turbine and V_ω is the wind speed. C_p wing pitch angle is the power coefficient of the wing which is a function of the β and the tip speed ratio.

$$C_P = k_1\left(\frac{k_2}{\lambda_i} - k_3\beta - k_4\beta^{k_5} - k_6\right)e^{-\left(\frac{k_7}{\lambda_i}\right)} \tag{5}$$

$$\lambda_i = \frac{1}{\lambda + k_8} \tag{6}$$

Here; β is the pitch angle and λ which is the tip speed ratio is found as follows;

$$\lambda_{opt} = \frac{\Omega_m R}{V_\omega} \tag{7}$$

Here; Ω_m is the mechanic angular speed.

B. THE DOUBLE FED INDUCTION GENERATOR DYNAMIC MODEL

The space vector algorithm contributes to the development of the generator by applying it to the basic electrical formulas while creating the αβ dynamic model of the system. In Figure 4, three different rotating reference frame typically used to develop the space vector based models of DFIG are shown. Space vector expressions could be attained from any one of these frames by using direct or inverse transformation [20].

$$\vec{V}_s^s = R_s \cdot \vec{i}_s^s + \frac{d\vec{\Psi}_s^s}{dt} \qquad \vec{V}_r^r = R_r \cdot \vec{i}_r^r + \frac{d\vec{\Psi}_r^r}{dt} \tag{8}$$

$$\vec{V}_s^s = R_s \cdot \vec{i}_s^s + \frac{d\vec{\Psi}_s^s}{dt} \Rightarrow \begin{cases} V_{\alpha s} = R_s \cdot i_{\alpha s} + \dfrac{d\Psi_{\alpha s}}{dt} \\ V_{\beta s} = R_s \cdot i_{\beta s} + \dfrac{d\Psi_{\beta s}}{dt} \end{cases} \tag{9}$$

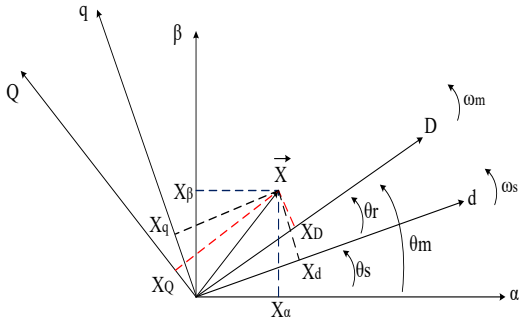

Figure 4. *The space vector graphics of DFIG in different reference frames*

$$\vec{V}_r^s = R_r \cdot \vec{i}_r^s + \frac{d\vec{\Psi}_r^s}{dt} - j\omega_m\vec{\Psi}_r^s$$
$$\Rightarrow \begin{cases} V_{\alpha r} = R_r \cdot i_{\alpha r} + \dfrac{d\Psi_{\alpha r}}{dt} + \omega_m\Psi_{\beta r} \\ V_{\beta r} = R_r \cdot i_{\beta r} + \dfrac{d\Psi_{\beta r}}{dt} - \omega_m\Psi_{\alpha r} \end{cases} \tag{10}$$

$$\vec{\Psi}_s^s = L_s \cdot \vec{i}_s^s + L_m \cdot \vec{i}_r^s \tag{11}$$

$$\Rightarrow \begin{cases} \Psi_{\alpha s} = L_s \cdot i_{\alpha s} + L_m \cdot i_{\alpha s} \\ \Psi_{\beta s} = L_s \cdot i_{\beta s} + L_m \cdot i_{\beta s} \end{cases}$$

$$\vec{\Psi}_r^s = L_m \cdot \vec{i}_s^s + L_r \cdot \vec{i}_r^s$$

$$\Rightarrow \begin{cases} \Psi_{\alpha r} = L_m \cdot i_{\alpha r} + L_r \cdot i_{\alpha r} \\ \Psi_{\beta r} = L_m \cdot i_{\beta r} + L_r \cdot i_{\beta r} \end{cases} \quad (12)$$

Here; v_s and v_r represents the stator and rotor voltage, R_s and R_r represents the stator and rotor resistances, ψ_s and ψ_r represents the stator and rotor fluxes. L_s, L_r and L_m are respectively the stator, rotor and their common inductances. αβ equivalent circuit of the equations has been developed as shown in Figure 5. Here it is seen that all magnitudes are sinusoidal at ω_s frequency. The power equations of the stator and rotor parts are as follows.

$$P_s = \frac{3}{2}\left(v_{\alpha s} i_{\alpha s} + v_{\beta s} i_{\beta s}\right) \qquad P_r = \frac{3}{2}\left(v_{\alpha r} i_{\alpha r} + v_{\beta r} i_{\beta r}\right) \quad (13)$$

$$Q_s = \frac{3}{2}\left(v_{\beta s} i_{\alpha s} - v_{\alpha s} i_{\beta s}\right) \qquad Q_r = \frac{3}{2}\left(v_{\beta r} i_{\alpha r} - v_{\alpha r} i_{\beta r}\right) \quad (14)$$

The electromagnetic torque formed by DFIG can be calculated as follows.

$$T_{em} = \frac{3}{2} p \mathrm{Im}\left\{\vec{\Psi}_r \vec{i}_r^*\right\} = \frac{3}{2} p\left(\Psi_{\beta r} i_{\alpha r} - \Psi_{\alpha r} i_{\beta r}\right) \quad (15)$$

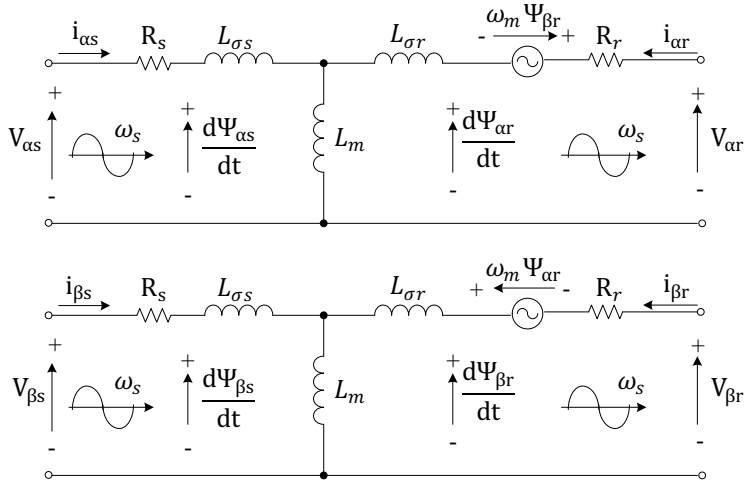

Figure 5. *αβ reference frame model of DFIG.*

$$\begin{aligned} T_{em} &= \frac{3}{2} p \frac{L_m}{L_s} \mathrm{Im}\left\{\vec{\Psi}_s \vec{i}_r^*\right\} = \frac{3}{2} p \mathrm{Im}\left\{\vec{\Psi}_s^* \vec{i}_s\right\} \\ &= \frac{3}{2} \frac{L_m}{L_r} p \mathrm{Im}\left\{\vec{\Psi}_r^* \vec{i}_s\right\} = \frac{3}{2} \frac{L_m}{\sigma L_r L_s} p \mathrm{Im}\left\{\vec{\Psi}_r^* \vec{\Psi}_s\right\} \\ &= \frac{3}{2} L_m p \mathrm{Im}\left\{\vec{i}_s \vec{i}_r^*\right\} \end{aligned} \quad (16)$$

Here; $\sigma = 1 - \frac{L_m^2}{L_s \cdot L_r}$.

In this way; if the Equations (9) and (12) are re-arranged, the following space vector equation formed with the combination of the stator and rotor fluxes is attained.

$$\frac{d}{dt}\begin{bmatrix}\vec{\Psi}_s^s\\ \vec{\Psi}_r^s\end{bmatrix}=\begin{bmatrix}\frac{-R_s}{\sigma L_s} & \frac{R_s L_m}{\sigma L_s L_r}\\ \frac{R_r L_m}{\sigma L_s L_r} & \frac{-R_r}{\sigma L_r}+j\omega_m\end{bmatrix}\begin{bmatrix}\vec{\Psi}_s^s\\ \vec{\Psi}_r^s\end{bmatrix}+\begin{bmatrix}\vec{v}_s^s\\ \vec{v}_r^s\end{bmatrix} \quad (17)$$

In this way, the mechanic movement equation defining the speed of the rotor is also as follows;

$$T_{em}-T_{load}=J\frac{d\Omega_m}{dt} \quad (18)$$

Here; J is the inertia coefficient of the motor, T_{load} mile is the applied load torque. As a result; the DFIG equations necessary to be able to prepare simulations on computer are attained.

C. CROWBAR

In Figure 6, the Crowbar section is connected between the rotor of the DFIG and the RSC inverter. Most of the manufacturers have suggested the use of IGBT instead of thyristor to ensure the rapid and direct turn off of the crowbar connection and also ensure the re-activation of RSC to continue to normal operation. If the rotor current or dc bus bar voltage levels exceed the limits, the IGBT triggers of RSC are cut off and crowbar is activated. Dc-bus bar voltage is examined during the crowbar movement. When this voltage is low enough, crowbar is separated.

Reactive power will be provided for the grid support by re-activating RSC after a little delay. Normally, Crowbar is disabled while RSC and GSC are running. In order to protect the rotor against high voltages when the voltage drop occurs, the crowbar switch is opened and excessive current flows from the RSC to the crowbar is prevented.

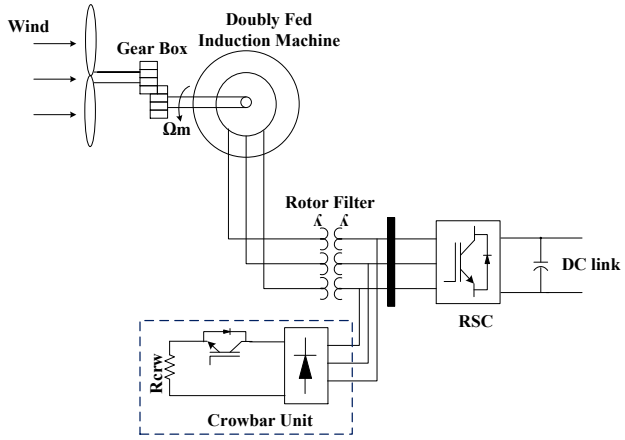

Figure 6. *Rotor crowbar protection circuit.*

D. DFIG CONTROL

Vector control for DFIG consists of traditional PI transformations and clarke / park transformations. Several publications on vector control of DFIG have also been published [21] and [22-23]. The vector control structure for DFIG is as follows.

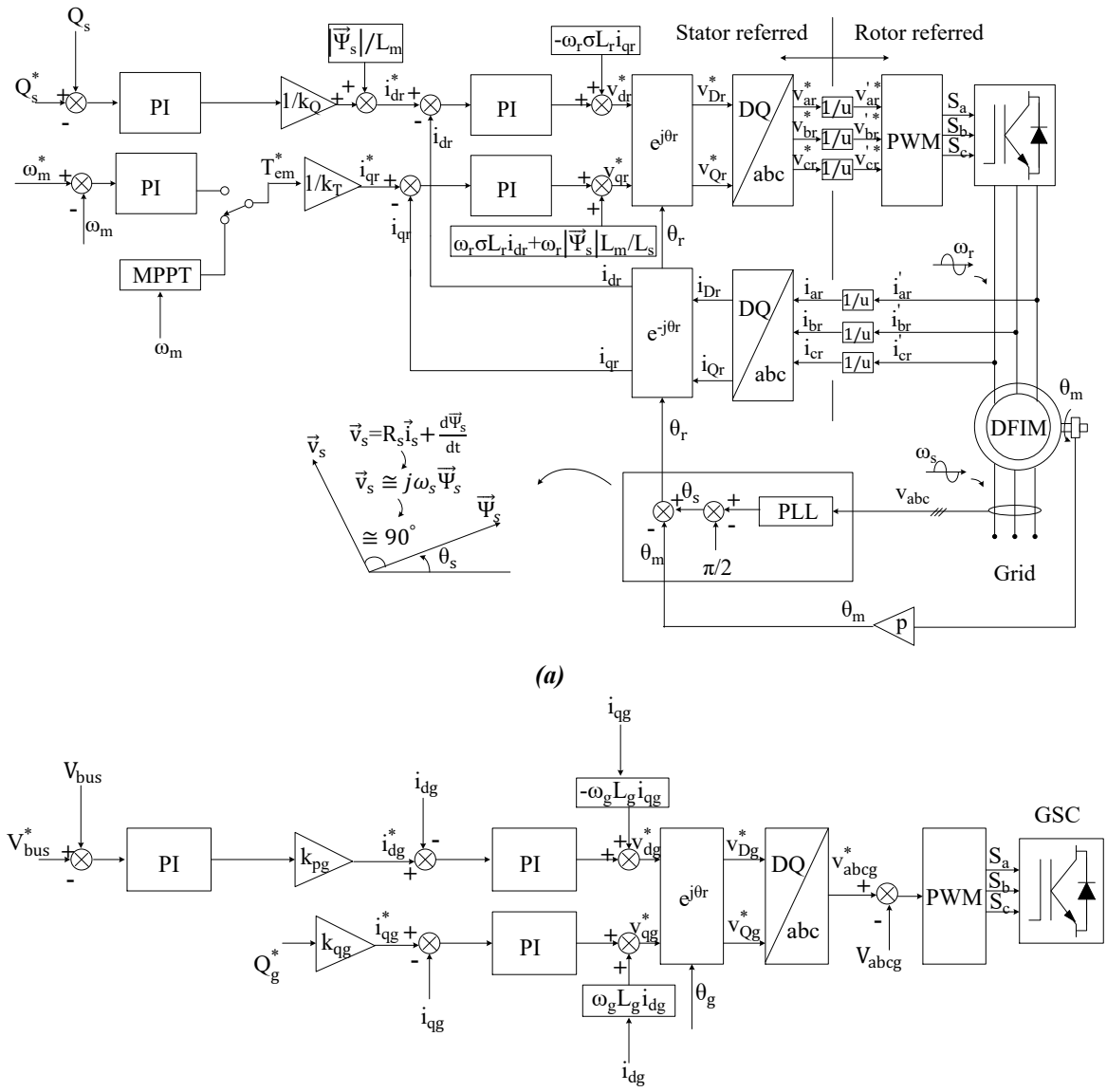

Figure 7. *DFIG vector control,* ***(a)*** *RSC control,* ***(b)*** *A part of GSC control.*

The vector control of DFIG was performed in the dq reference frame. RSC consists of a speed, torque and current loop. The torque and reactive power of the generator are controlled by the vector control of the inverter on the rotor side. The reference i^*_{qr} rotor current is obtained by setting the reference torque equation.

In this study, the reference torque T^*_{em} is calculated using MPPT. The reference i_{dr}* rotor current is obtained by regulating the reactive power generated by DFIG as in Figure 7 (a). The purpose of the grid side control is to keep the dc bus voltage constant regardless of the upper and lower synchronous operating range. The voltage equation in the synchronous reference frame can be expressed as follows.

$$\begin{aligned} v_{dr} &= R_r i_{dr} + \sigma L_r \frac{d}{dt} i_{dr} - \omega_r \sigma L_r i_{qr} + \frac{L_m}{L_s} \frac{d}{dt} \left|\vec{\Psi}_s\right| \\ v_{qr} &= R_r i_{qr} + \sigma L_r \frac{d}{dt} i_{qr} + \omega_r \sigma L_r i_{dr} + \omega_r \frac{L_m}{L_s} \left|\vec{\Psi}_s\right| \end{aligned} \tag{19}$$

Figure 7 (b) shows the grid side control. The reference d-axis i_{dg}* is calculated by applying a PI

controller on the DC bus voltage v_{dc}; where q-axis reference current (i_{qg}*) representing reactive power is given to zero. The reference voltage (V^*_{GSC}) is calculated by using (19) for GSC to control the current cycles.

All control systems may be carried out after the flux angle and current control calculation. Since the d axis in the reference frame is in the same plane as the stator flux, the torque equation in dq reference frame can be written as follows:

$$T_{em} = \frac{3}{2} p \frac{L_m}{L_s} (\Psi_{qs} i_{dr} - \Psi_{ds} i_{qr})$$
$$\Rightarrow T_{em} = \frac{3}{2} p \frac{L_m}{L_s} |\vec{\Psi}_s| i_{qr} \Rightarrow T_{em} = K_T i_{qr} \quad (20)$$

It is understood that the q-axis rotor current component is proportional to the torque; in other words, it is possible to control i_{qr} and torque and therefore, it also means that the speed of the machine could be controlled when necessary. Similarly; the stator reactive power statement in dq frame could be developed and a compact statement revealing that i_{dr} is responsible for Q_s could be attained.

$$Q_s = \frac{3}{2} (v_{qs} i_{ds} - v_{ds} i_{qs})$$
$$\Rightarrow Q_s = -\frac{3}{2} \omega_s \frac{L_m}{L_s} |\vec{\Psi}_s| \left(i_{dr} - \frac{|\vec{\Psi}_s|}{L_m} \right) \quad (21)$$
$$\Rightarrow Q_s = K_Q \left(i_{dr} - \frac{|\vec{\Psi}_s|}{L_m} \right)$$

In selected orientations, it is seen that the rotor current can be controlled independently. According to these expressions, Figure 8 shows the general vector control of the system.

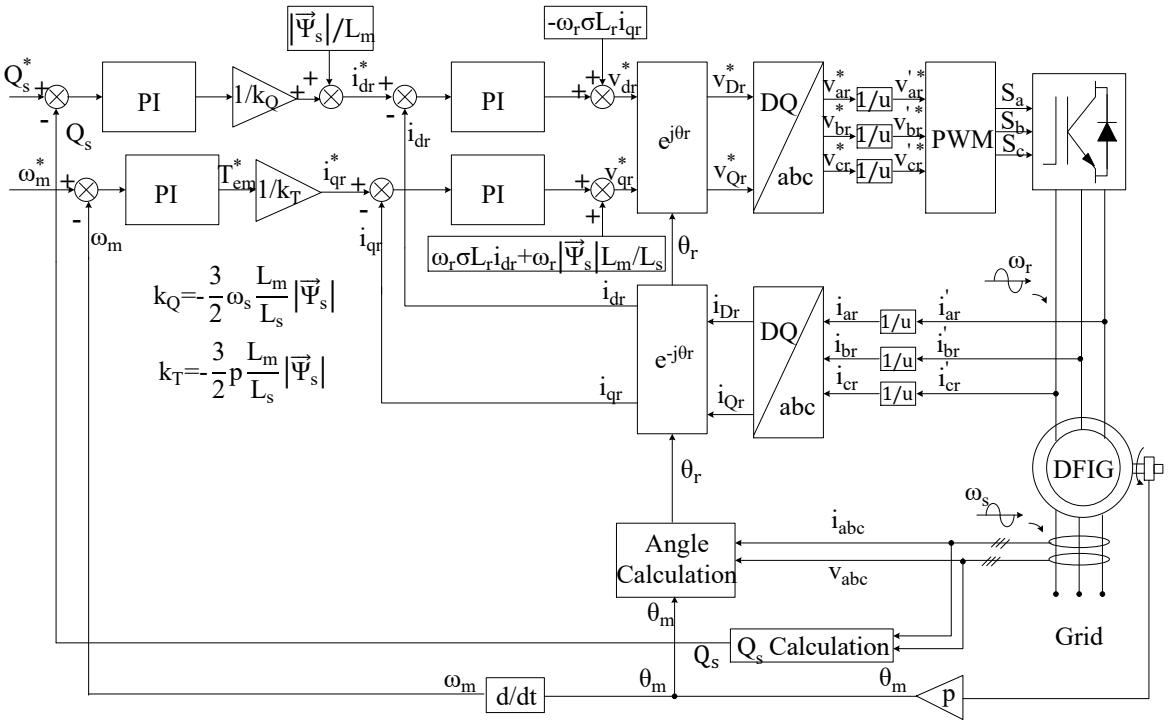

Figure 8. *DFIG vector control complete circuit model.*

E. ANALYSIS OF DFIG IN VOLTAGE DIPS

Voltage dips are known as the sudden grid voltage drops stemming from unexpected phenomena or

failures occurring in the mains. When a voltage dip is observed by a direct DFIM stator, it is necessary to analyze the behavior of the stator flux to understand the hardships stemming from the distortion caused by the dip. In this way, the following statement is attained by combining the voltage and rotor flux statements and extracting the stator current:

$$\frac{d\vec{\Psi}_s^s}{dt} = \vec{v}_s^s - \frac{R_s}{L_s}\vec{\Psi}_s^s + R_s\frac{L_m}{L_s}\vec{i}_r^s \tag{22}$$

When a sudden voltage dip occurs, it is understood that the stator flux cannot come to the stable state as fast as the stator voltage. Every phase of stator flux develops as an exponential which is the total of a sinusoid and whose time constant is Ls / Rs. The term rotor current may ensure the flux to decrease in a faster way. It is necessary not to forget that the rotor current is controlled via the rotor side converter as long as the control is not lost. It is possible to attain the following equation from the voltage and flux equations.

$$\vec{v}_r^r = \frac{L_m}{L_s}\left(\vec{v}_s^r - j\omega_m\vec{\Psi}_s^r\right) + \left[R_r + \left(\frac{L_m}{L_s}\right)^2 R_s\right]\vec{i}_r^r + \sigma L_r\frac{d}{dt}\vec{i}_r^r \tag{23}$$

The rotor voltage can be divided into two parts. The first is the electromotive force generated in the rotor due to stator flux. The other part could be handled as the voltage dip in both the resistance and temporary inductance.

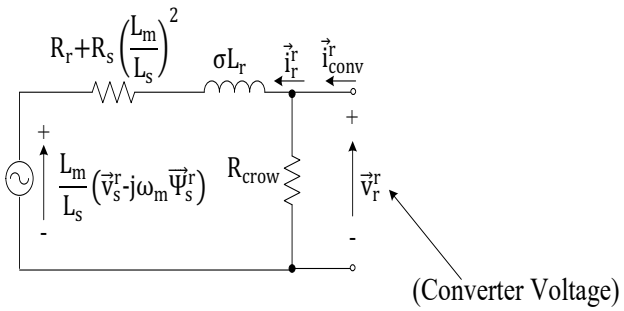

Figure 9. *The equivalent circuit of DFIM for the analysis of the voltage dips.*

Control must not be lost to keep rotor currents within safe limits. This requires an exceptionally higher rotor voltage amplitude at the start of the voltage level. This situation causes the rotor side control output voltage to rise due to the high rotor electromotor force when the grid fault occurs. In such events, it is best to turn off the RSC. This is done by turning off the crowbar. Figure 9 shows the electrical circuit of a crowbar and rotor side equivalent circuit.

III. SIMULATION RESULTS AND DISCUSSION

In the conducted simulation study, the connection of DFIG to the grid has been realized by conducting the synchronization of the stator voltage of DFIG widely used in the wind turbines with the grid voltage with the help of MATLAB&Simulink program. Parameters belonging to the turbine used in the simulation are given in Table 1. The parameters belonging to the crowbar unit used, DC bus bar condenser, grid filter and DFIG are given in the simulation in Table 2. The DFIG connected to the grid has been firstly operated without any protection unit and the rotor and stator graphics have been attained. After that, the occurring reactions have been analyzed when grid failure occurs. Grid voltage has been decreased to the level of 10% at the 3rd second. Afterwards, it has been increased as ramp in a way that it will be 15 pu per second until the seconds of 3.5 and 4.17. The grid voltage graphics regarding the conducted scenario is seen in Figure 10.

Table 1. *Simulation parameters of Turbine.*

Parameters	Value	Unit
Radius	42	m
Nominal wind speed	12.5	m/s
Variable speed ratio	9-18	rpm
Optimum tip speed ratio λ_{opt}	7.2	-
Maximum power coefficient C_{p_max}	0.44	-
Air density ρ	1.225	kg/m^3

Table 2. *Simulation parameters of DFIG and others.*

Main Characteristics of the Generator	Value	Unit
Nominal stator active power	2.0	MW
Nominal Torque	12732	Nm
Stator Voltage	690	V
Nominal Speed	1500	Rpm
Stator current	1760	A
Speed Range	900-2000	Rpm
Pole Pairs	2	-
Ratio (u)	1/3	-
Rotor voltage	2070	V
smax	1/3	-
Rs	2.6	mΩ
Lsi	0.087	mH
Lm	2.5	mH
Ls	Lm+Lsi	mH
Lr	Lm+Lsi	mH
Rr	2.9	mΩ
Vbus	1150	V
Inertia	127	Kg.m^2
Friction factor	0.001	N.m.s
Switching frequency	4000	Hz
Sampling time	5	µs
Cbus	80	mF
Rg(grid filter resistance)	20	µΩ
Lg(grid filter inductance)	400	µH
Crowbar resistance	0.2	Ω

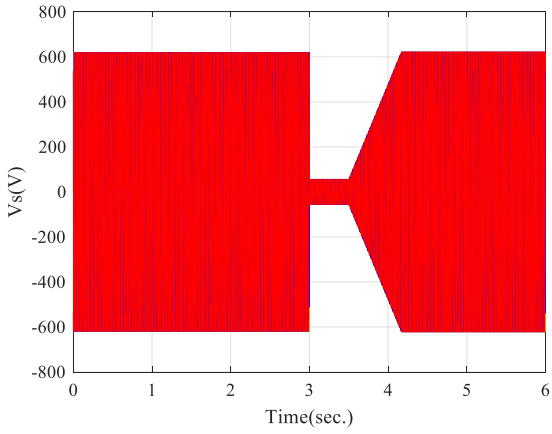

(a)

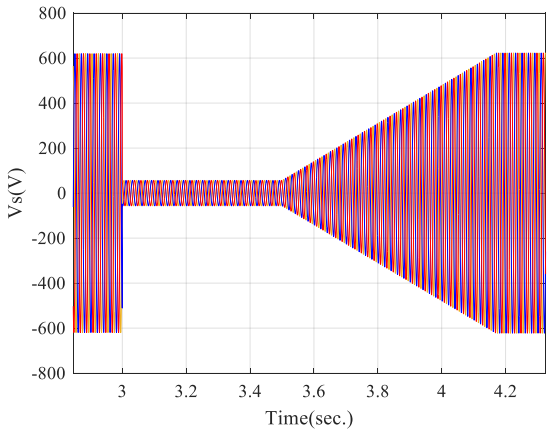

(b)

Figure 10. *Grid voltage,* ***(a)*** *voltage dip,* ***(b)*** *voltage dip zoom.*

Crowbar unit is suddenly activated at the moment when there is voltage dip and all the current is transmitted on the energy crowbar resistance. Therefore; the selection of this resistance has great significance. There are many studies in the literature regarding the selection of the crowbar resistance. The following Figure 11 shows the rotor speed graphics belonging to the situations in which there is a failure, there is a crowbar unit and there is no crowbar unit. No reference speed has been given to the system. 8.5 m/s has been stabilized as the wind speed. According to this speed value, MPPT algorithm produces a torque reference. This reference has been adapted to the system with a controller by comparing the q compound current coming from the feedback with torque. It is seen in the graphics that the speed value has shown a little more overflow while there is crowbar unit. The reason for this is that RSC unit is deactivated at the moment of protection. Besides, a purer speed curve with no oscillation is observed at the moment of protection.

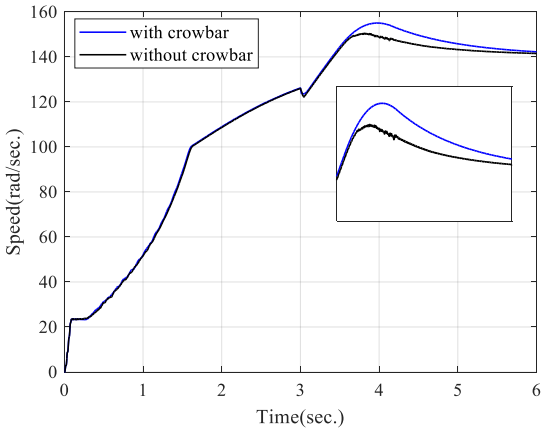

Figure 11. *Rotor speed with crowbar and without crowbar.*

The current graphics in d and q reference roof are seen in Figure 12. The state with and without crowbar has been given comparatively in the graphics here. The crowbar IGBT switch is triggered and activated in 3rd second. Crowbar unit remains active for 0.1 seconds and it is made passive by opening the switch in 3.1st second. Rotor side inverter is also activated until the 3rd second and it is also deactivated in 3.1st second. Namely; RSC works up to 0.1 seconds. In this way, all the current has flowed upon the crowbar resistance and it protected the RSC unit against the over current and other negative impacts. It is also clearly seen in the graphics that the reference currents of the control with crowbar could trace the currents much better.

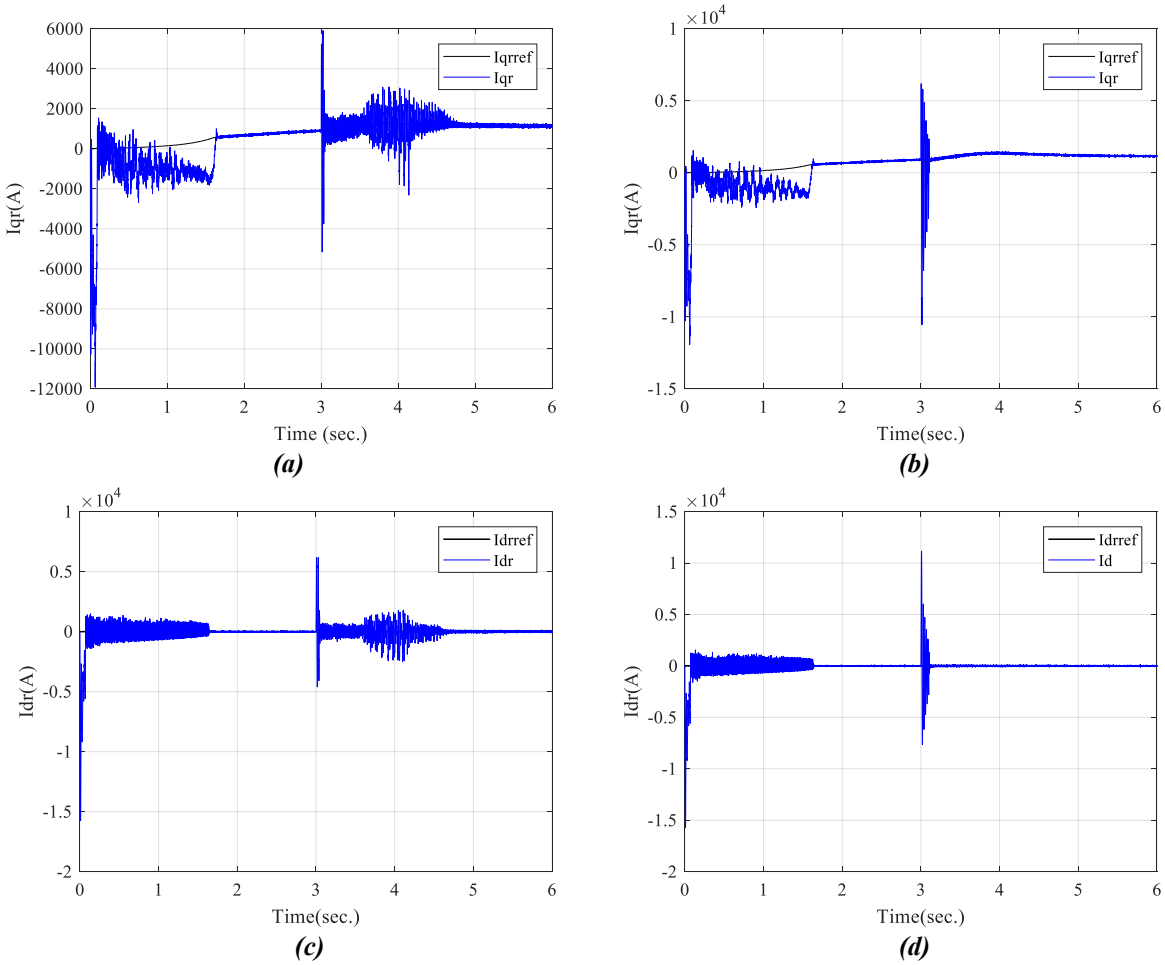

Figure 12. *d and q axis rotor current with crowbar and without crowbar, a) q-axis rotor current without crowbar,b) q-axis rotor current with crowbar, c) d-axis rotor current without crowbar, d) d-axis rotor current with crowbar.*

Figure 13 shows the comparative results of the torque graph obtained from the feedback versus the reference torque component produced by the MPPT algorithm. Here the torque from the feedback appears to follow the reference torque quite well in the crowbar unit. When the voltage dip occurs in the 3rd second, the torque settled to a value of 0 by making a peak. This is due to the fact that the RSC is disconnected and can no longer track the maximum power.

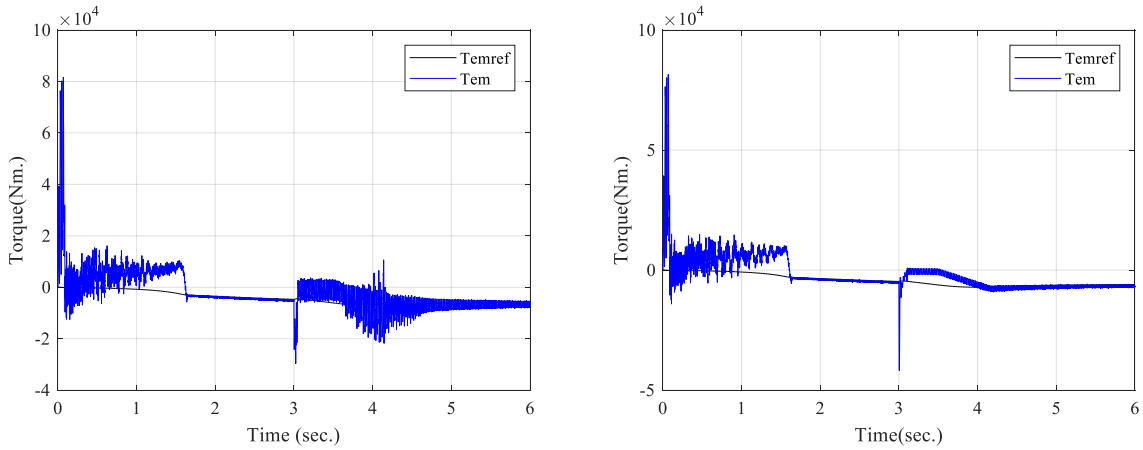

Figure 13. *Electromagnetic torque with crowbar and without crowbar,* ***(a)*** *without crowbar,* ***(b)*** *with crowbar.*

The comparative analyses with and without crowbar belonging to the stator and rotor currents are given in Figure 14. When the detailed images are paid attention, how the crowbar unit protects the rotor against harmonic currents is clearly seen.

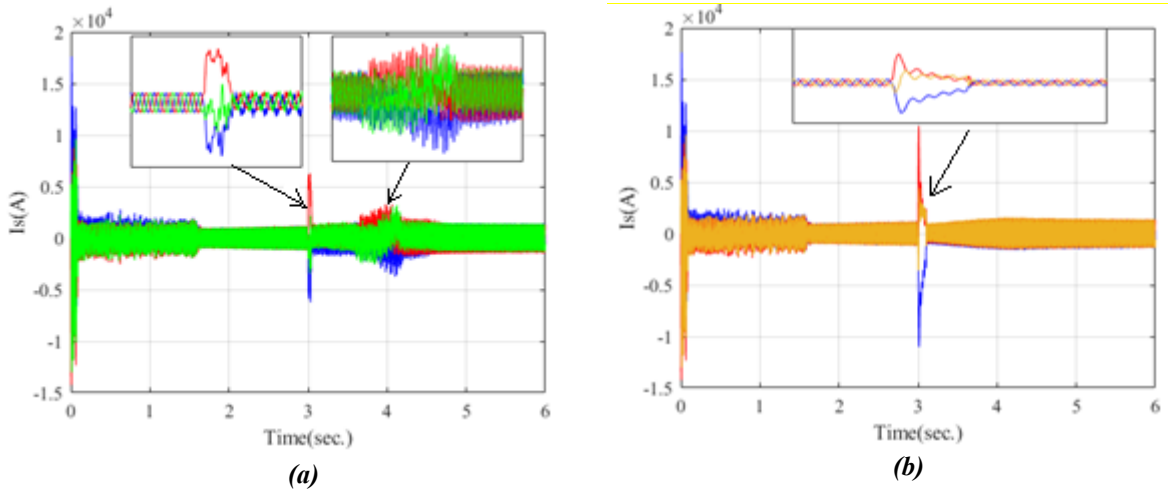

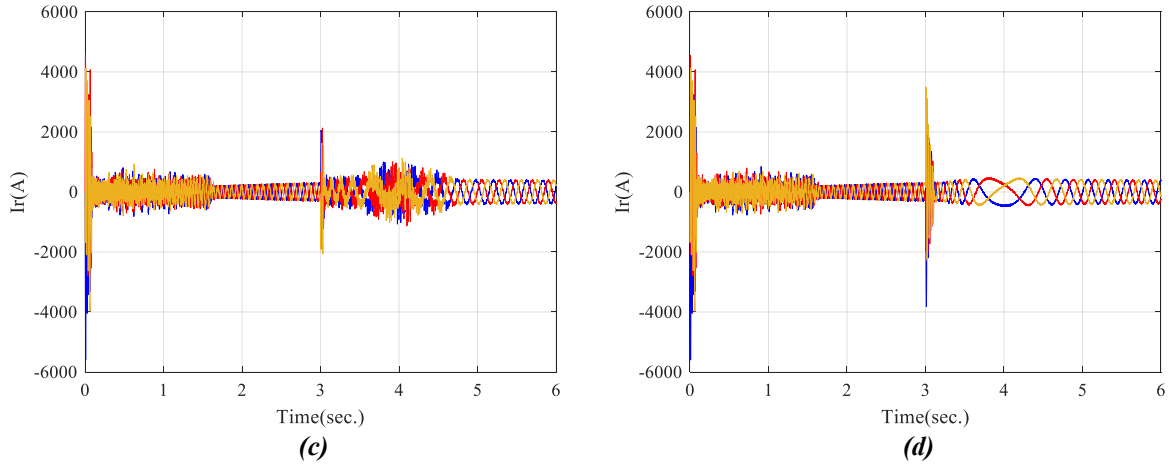

Figure 14. *Three phase stator and rotor currents with crowbar and without crowbar,* ***(a)*** *stator current without crowbar,* ***(b)*** *stator current with crowbar,* ***(c)*** *rotor current without crowbar,* ***(d)*** *rotor current with crowbar.*

The reaction of DC bus bar voltage with and without crowbar is seen in Figure 15. DC bus bar has shown a great excess and raised to uncontrollable values when there is no crowbar in the system when 3rd second voltage dip has occurred. 4.17th second could just catch the reference value when the grid voltage has decreased to the normal value. However; when crowbar has been used, crowbar has been activated at the moment of voltage dip and has ensured the dc bus bar voltage to remain in the reference value.

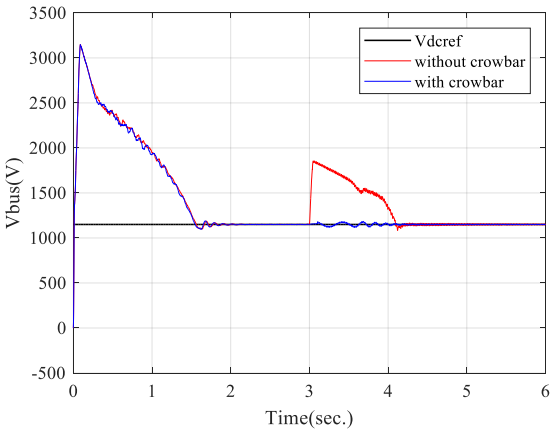

Figure 15. *DC link voltage with crowbar and without crowbar.*

d and q compounds of the grid currents are seen in Figure 16. d current compound has passed to the negative zone when DC bus bar voltage has come to the reference value. This means that active power has been given to the grid by the generator. It has caught its reference value again with a little oscillation while there is crowbar at the moment of failure. However; generator has been deactivated and motor has been operated in the control without crowbar. d current has passed to the positive side and given active power to the motor. It is seen that q current compound has followed the value of 0 given as reference. There is a small reactive power attraction at the moment of failure. However; the system has gathered itself up rapidly and turned back to the reference value.

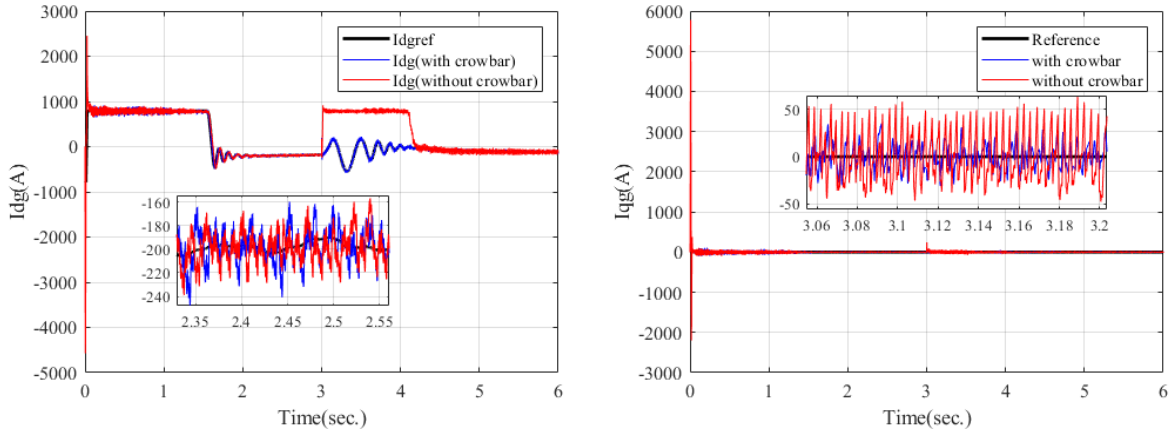

Figure 16. *Grid side d and q current with crowbar and without crowbar.*

Grid and generator single phase sinusoidal voltage signals during the synchronization are given in Figure 17. It is seen here that the grid and generator voltages are synchronized per approximately 1.63 seconds. When dc bus bar voltage value reaches the reference value, d voltage compounds have settled on 0 value. The reason why d voltage values are stable at 0 shows that the system has reached the synchronous operational point. This shows us that the system is out of the synchronous operation. q current compound to remain in positive value means the grid does not attract any reactive power and this power is transmitted to generator.

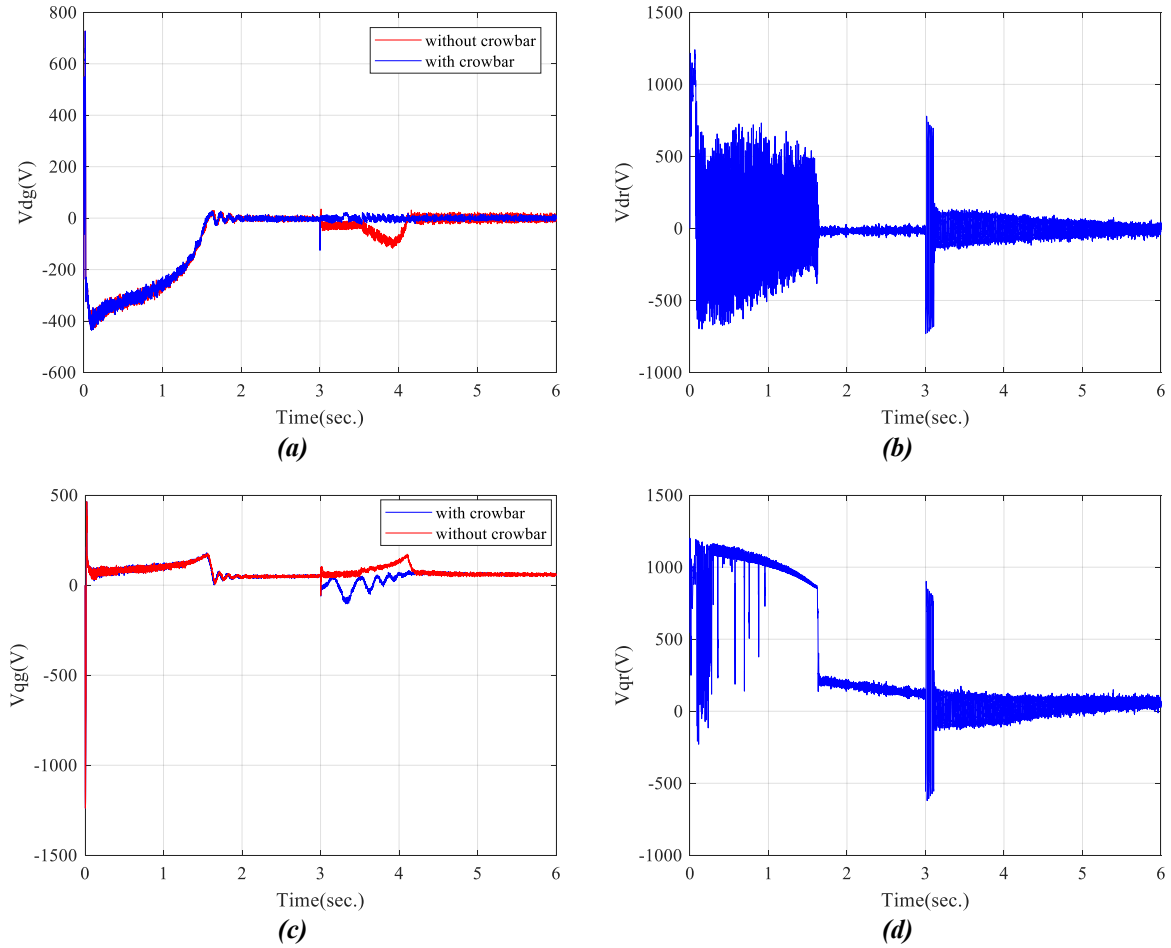

Figure 17. *Grid and generator d and q voltage components with crowbar and without crowbar* ***(a)*** *d-axis grid voltage,* ***(b)*** *d-axis rotor voltage,* ***(c)*** *q-axis grid voltage,* ***(d)*** *q-axis rotor voltage.*

Three phase current graphics belonging to the grid are seen in Figure 18. The grid current has been tried to be taken to minimum levels at the failure moment due to the use of Crowbar. However; when crowbar is not used, the grid current continues its path with the stable failure current at the moment of failure and brings negative impacts on the system.

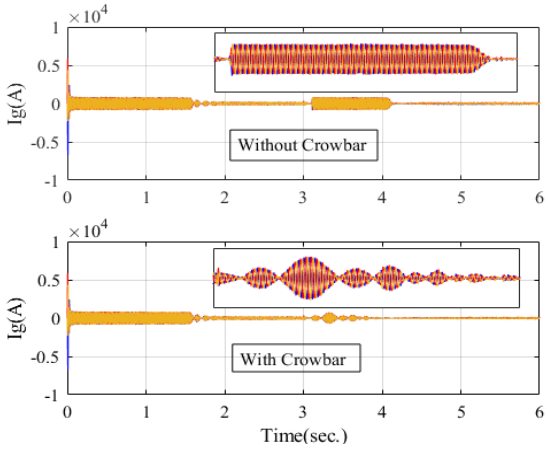

Figure 18. *Three phase grid current with crowbar and without crowbar.*

The current graphics occurring on crowbar resistance at the moment of failure is seen in Figure 19. The current has reached the peak value and turned to the zero value again within 0.1 second interval; because, the crowbar unit has been activated for 0.1 seconds. In this way, this harmful current has been demolished on crowbar unit without giving it to the system.

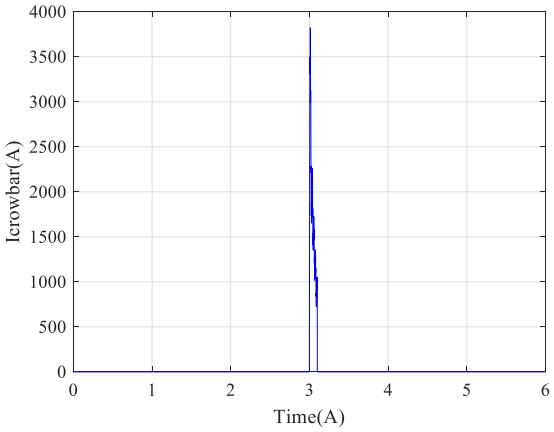

Fiure. 19. *Crowbar resistance current.*

IV. CONCLUSION

Low voltage problem for DFIG wind turbines is a hardship necessary to be solved by the manufacturers and users in all implementations. There are many low voltage rehabilitation techniques (LVRT) in the literature for this. However; this method has not been handled comprehensively. It is necessary to pay so much attention to the location, period, failure type and reactive power compensation method of the failure to be able to get full efficiency from a wind turbine. A crowbar protection system could be operated to prevent strong currents flowing in the rotor and distribute unnecessary active power. However; together with the activation of crowbar, DFIG will lose its ability to control the reactive power and turn into a squirrel-cage asynchronous generator. At the same time, it is necessary to choose the resistance value used in the crowbar unit very well; because, all the energy flows on this resistance at the moment of failure. This value is suggested to be minimum 20 times more than the rotor resistance

in the literature. In this study, the reaction of DFIG wind turbine has been analyzed at the moment of grid voltage dip. DFIG rotor currents, stator currents, grid voltage and currents, rotor speed and DC-bus bar voltage have been monitored continuously and under the conditions of failure. Detailed graphics have been given by examining the analyses such as the use and non-use of crowbar, activation time and deactivation time. The dynamic simulation results conducted on the wind turbine show that the control method gives very good reaction under the conditions such as low voltage failure and protect the system against the high rotor currents.

V. REFERENCES

[1] J.Arbi, M.Ghorbal, I.Belkhodja and L.Charaabi, "Direct virtual torque control for doubly fed induction generator grid connection," *IEEE Transactions on Industrial Electronics.* vol. 56, no.10, pp. 4163-4173, 2009.

[2] L. Shuhui, and T. A. Haskew, "Characteristic study of vector-controlled doubly-fed induction generator in stator-flux-oriented frame," *Electric Power Components and Systems*, pp. 990-1015, 2008.

[3] B.H. Chowdhury and S. Chellapilla, "DFIG control for variable speed wind power generation," *Electric Power System Research*, vol. 76 pp. 786-800, 2006.

[4] R. Fadaeinedjad, M. Moallem and G. Moschopoulos, "Simulation of a wind turbine with DFIG by FAST and Simulink." *IEEE Transactions on Energy Conversion*, vol. 23, no.2, pp. 690-700, 2008.

[5] Y. Wang, D. Zhao, B. Zhao and H. Xu, "A new type of control strategy of DFIG in wind power system based on SMC," *International Conference on Electrical Machines and Systems*, pp. 2428-2431, 2008.

[6] W. Guo, L. Xiao, S. Dai, Y. Li, X. Xu, W. Zhou and L. Li, "LVRT capability enhancement of DFIG with switch-type fault current limiter," *IEEE Transactions on Industrial Electronics*, vol. 62, no.1, pp. 332-342, 2014.

[7] J. Lopez, E. GubÍa, P. Sanchis, X. Roboam and L Marroyo, "Wind turbines based on doubly fed induction generator under asymmetrical voltage dips," *IEEE Transactions on EnergyConversion,* vol. 23, no. 1, pp. 321-330, 2008.

[8] M. Mohseni S. M. Islam, and S. Masoum, "Impacts of symmetrical and asymmetrical voltage sags on DFIG-Based wind turbines considering phase-angle jump, voltage recovery, and sag parameters," *IEEE Transactions on Power Electronics*, vol.26, no.5, pp.1587-1598, 2011.

[9] P. Makolo, J. J. Justo, F. Mwasilu, and R. Zamora, "Fault ride through technique for DFIG based wind turbines under grid three-phase faults, *In 2018 Australasian Universities Power Engineering Conference (AUPEC)*, 2018, pp. 1-5.

[10] J. Lopez, E. Gubia, E. Olea, J. Ruiz, L. Marroyo, "Ride Through of Wind Turbines With Doubly Fed Induction Generator Under Dismetrical Voltage Dips." *IEEE Transactions on Industrial Electronics.* vol. 56, no. 10, pp. 4246-4254, 2009.

[11] D. Xie, Z. Xu, L. Yang, J. Østergaard, Y. Xue and K. P. Wong, "A comprehensive LVRT control strategy for DFIG wind turbines with enhanced reactive power support." *IEEE Transactions on Power Systems,* vol.28, no.3, pp. 3302-3310, 2013.

[12] H. Geng, C. Liu and G. Yang, "LVRT capability of DFIG-based WECS under asymmetrical Grid fault condition," *IEEE transactions on Industrial electronics*, vol.60, no.6, pp.2495-2509, 2012.

[13] W. Wang, M. Sun, and X. Zhu, "Analysis on the Low Voltage Ride Through Technology of DFIG [J]." *Automation of Electric Power Systems*, 2007, 23.

[14] J. J. Justo, and F. A. Mwasilu, "Low voltage ride through enhancement for wind turbines equipped with DFIG under symmetrical grid faults." *Tanzania Journal of Engineering and Technology*, vol.37, no.2, 2019.

[15] P. Mukherjee and V. V. Rao, "Superconducting magnetic energy storage for stabilizing grid integrated with wind power generation systems." *Journal of Modern Power Systems and Clean Energy*, vol.7, no.2, pp.400-411, 2019.

[16] Q. U. Yanbin, G. A. O. Le, M. A. Guangfu, S. O. N. G. Huihui and W. A. N. G. Shitao, "Crowbar resistance value-switching scheme conjoint analysis based on statistical sampling for LVRT of DFIG," *Journal of Modern Power Systems and Clean Energy*, vol.7, no.3, pp.558-567, 2019.

[17] F. A. N. Zhanfeng, S. O. N. G. Guobing, K. A. N. G. Xiaoning, T. A. N. G. Jisi, and W. A. N. G. Xiaobo, "Three-phase fault direction identification method for outgoing transmission line of DFIG based wind farms." *Journal of Modern Power Systems and Clean Energy*, vol.7, no.5, pp.1155-1164, 2019.

[18] A. H. Kasem, E. F. El-Saadany, H. H. El-Tamaly and M. A. A. Wahab, "An improved fault ride-through strategy for doubly fed induction generator-based wind turbines." *IET Renew. Power Gener.,* vol. 2, no. 4, pp. 201-214, 2008.

[19] A. D. Hansen, P. Sørensen, F. Iov and F. Blaabjerg, "Control of variable speed wind turbines with doubly-fed induction generators. *Wind Eng.,* vol. 28, no. 4, pp. 411-432, 2004.

[20] Y. Lei, A. Mullane, G. Lightbody and R. Yacamini, "Modeling of the wind turbine with a doubly fed induction generator for grid integration studies." *IEEE Trans. Energy Convers.,* vol. 21, no. 1, pp. 257–264, 2006.

[21] R. Pena, J. C. Clare and G. M. Asher, "Doubly fed induction generator using back-to-back PWM converters and its application to variable-speed wind-energy generation." *IEE Proc.-Electr. Power Appl.,* vol. 143, no. 3, pp. 231-241, 1996.

[22] Z. Rafiee, S. S. Najafi, M. Rafiee, M. R. Aghamohammadi and M. Pourgholi, "Optimized control of Coordinated Series Resistive Limiter and SMES for improving LVRT using TVC in DFIG base wind farm," *Physica C: Superconductivity and its Applications*, 570, 1353607, 2020.

[23] A. T. Nguyen, and D. C. Lee, (2020, October). "LVRT Control based on Partial State Feedback Linearization for SCIG Wind Turbine Systems." *In 2020 IEEE Energy Conversion Congress and Exposition (ECCE),* 2020, pp. 93-98.

[24] X. Yifan, A. Aimin, Z. Yingying and C. Wei, "Design and Implementation of Crowbar Circuits Combined with Chopper Circuits for LVRT in Wind Farms." *In Journal of Physics: Conference Series,* vol. 1639, no. 1, pp. 012040, 2020.

[25] M. A. S. Ali, K. K. Mehmood, S. Baloch and C. H. Kim, "Modified rotor-side converter control design for improving the LVRT capability of a DFIG-based WECS." *Electric Power Systems Research,* 186, 106403, 2020.

[26] M. Firouzi, "Low-voltage ride-through (LVRT) capability enhancement of DFIG-based wind farm by using bridge-type superconducting fault current limiter (BTSFCL)." *Journal of Power Technologies,* vol.99, no.4, pp.245-253, 2020.